Studies of HBr Uptake on Ice Films at 188 K

Liang T. Chu* and Liang Chu

Wadsworth Center and Department of Environmental Health and Toxicology, State University of New York, Albany, New York 12201-0509

Received: August 13, 1998; In Final Form: November 3, 1998

The interaction of HBr with ice films has been studied in a fast-flow reactor, and the formation of $HBr\cdot 3H_2O$ and $HBr\cdot 2H_2O$ near the ice film surface was determined at 188 K. The existence of the hydrates was further verified by the construction of a low-temperature HBr−ice phase diagram under the experimental conditions. Hydrate formation is a critical process in understanding the higher HBr uptake on ice films and the heterogeneous reaction mechanism involving HBr on the ice surface. The effects of total pressure and ice film thickness on HBr uptake were also investigated. The co-uptake of HBr and HCl showed that the HBr uptake was in general more efficient than that of HCl. This study provides the detailed thermodynamic properties of HBr on ice at the pressure range of 10^{-8} -10^{-5} Torr and 180−220 K.

I. Introduction

Bromine and chlorine species are known to interact with ozone in the stratosphere and troposphere.[1−5] Bromine is also recognized to have a higher capacity to deplete ozone than chlorine on a per atom basis in the lower stratosphere.[4] The heterogeneous reactions involving photochemically inactive chlorine species on polar stratospheric clouds (PSCs) have become well recognized following the discovery of the Antarctic ozone hole.[6−8] There are two main classes of PSCs: type I, which consists of nitric acid−ice composed of mainly the trihydrate and dihydrate, and type II, consisting of water ice with small amounts of acidic impurities. These heterogeneous interactions are typically involved with gaseous species occurring on either cloud surfaces or aerosols. A typical reaction in the polar ozone chemistry is

$$ClONO_2 + HCl(s) \rightarrow Cl_2 + HNO_3(s) \qquad (1)$$

This reaction converts the reservoir compounds ($ClONO_2$ and HCl) into photochemically active species on PSC surfaces. The general consensus about the bromine reservoir compounds (e.g., HBr, $BrONO_2$) is that they are less stable than chlorine reservoir species and, thus, their lifetimes are shorter. In the gas phase, they are readily photodissociated by solar radiation. The concentration of bromine compounds is lower than that of chlorine species. However, recent modeling and laboratory studies show that heterogeneous reactions such as

$$BrONO_2 + H_2O(s) \rightarrow HOBr + HNO_3(s) \qquad (2)$$

$$HOCl + HBr(s) \rightarrow BrCl + H_2O(s) \qquad (3)$$

not only activate bromine species but also have the ability to change the partitioning of other constituents.[9−11]

The importance of heterogeneous bromine chemistry is also reflected in understanding the sudden Arctic tropospheric boundary-layer ozone depletion located near ground-level snow/ice in the early springtime.[12−14] Understanding the interaction of HBr with ice is an initial step toward understanding those heterogeneous reactions occurring near the ice surface. It is a necessary step in understanding the reaction mechanism of HBr-containing heterogeneous reactions.

For simplicity in experimental approach, ice films are used in the laboratory to mimic type-II PSCs. Hanson and Ravishankara[15] studied the uptake of HBr on ice. They determined HBr surface concentrations as high as $\sim 5 \times 10^{15}$ molecules/cm^2 at 201 K and a partial HBr pressure of 4.2×10^{-7} Torr. This large uptake (~10 times the monolayer coverage) suggests the possible formation of a phase other than an HBr-in-ice solid, or the possible multilayer HBr adsorption on ice. Abbatt[16] found that the uptake of HBr on ice is larger than 5×10^{16} molecules/cm^2 at an HBr pressure of 1.2×10^{-4} Torr and 228 K with an ice film thickness of a few tenths of a millimeter. Chu and Heron[17] studied the uptake of HBr on ice films as a function of partial HBr pressures and ice film temperatures. The uptake was determined to be in the range of $1.1 \times 10^{14} - 7.7 \times 10^{16}$ molecules/cm^2 at 188 and 195 K as HBr partial pressures varied from 3.7×10^{-8} to 6.4×10^{-6} Torr. The higher uptake amount is believed to be related to the formation of hydrobromic acid hydrates on ice films. The purpose of this study is to extend our preliminary study of HBr uptake on ice films and to characterize and reveal the nature of hydrates from the thermodynamic standpoint.

The identification of hydrobromic acid hydrates was reported mainly at about 100 K. The infrared spectrum of HBr hydrates was obtained by Delzeit et al.[18] at below 120 K and Gilbert and Sheppard[19] at about 200 K. Delzeit et al. also provided the detailed spectroscopic assignments of the hydrates. Lungdren[20] determined the single-crystal structure of hydrobromic acid monohydrate, dihyrate, and trihyrate at 91, 83, and 211 K, respectively. More recently, Rieley et al.[21] employed the molecular beam scattering technique to study the sticking coefficients of HBr and HCl on ice at 80−130 K and high-vacuum conditions. They determined the sticking probability of HBr on ice to be 1.00 ± 0.05 and HCl on ice to be $0.95 \pm$

* Author to whom correspondence should be addressed. Fax: (518) 473-2895. E-mail: lchu@cnsvax.albany.edu.

10.1021/jp9833799 CCC: $18.00
Published on Web 01/05/1999

0.05. After the sticking probability experiment, an FT-IR spectroscopic method was used to identify $(H_2O)_nH_3O^+$ as the main IR-active species present on the surface. Adsorbed HBr and HCl are exclusively ionic in nature.

In this study, we examine the interaction of HBr on ice surfaces under simulated polar atmospheric temperature, motivated by the potential importance of bromine heterogeneous chemistry in both the stratosphere and troposphere and the fundamental understanding of interaction of HBr on ice at lower temperatures. First, we will briefly describe the experimental apparatus and approach. Second, new experimental results will be presented, including the HBr uptake as a function of the total pressure and ice film thickness; detailed thermodynamic studies of HBr hydrates and the HBr−ice phase diagram at the polar atmospheric temperature. Finally, we will present the competitive co-uptake data of HBr and HCl on ice at 188 K.

II. Experimental Section

The uptake experiment was carried out in a tubular flow reactor and the loss of HBr into the ice film was monitored by a differentially pumped quadrupole mass spectrometer (QMS). The experimental apparatus was described earlier.[17,22] We will include here only those details related to the current study.

Flow Reactor. The borosilicate flow reactor was 35 cm in length with an inner diameter of 1.7 cm. The temperature in the reactor was regulated with a liquid-nitrogen-cooled methanol circulator and controlled with a digital temperature controller (Neslab). The mean temperature of the reactor was measured with two J-type thermocouples located at the middle and downstream end of the reactor, respectively. During the experiment, the temperature was maintained within ±0.3 K. The pressure inside the reactor was monitored by a high-precision pressure gauge (MKS Instruments, Model 690A, 10 Torr full scale), which was located at the downstream end of the flow reactor.

A quadrupole mass spectrometer (Extrel, C-50 electronics with 3/4 in. quadrupole rods) was housed in a differentially pumped ultrahigh vacuum (UHV) chamber. The background pressure in the chamber was $\sim 6 \times 10^{-11}$ Torr. This low background pressure ensured that the detection limit of the QMS in this system was as low as 2×10^{-8} Torr (7×10^8 molecules/cm^3) for HBr. The UHV chamber consisted of two stages: a differential pumping stage and a detection stage, which was pumped with a Varian VHS-4 diffusion pump and a titanium sublimation pump. These two stages were separated by a molecular-beam skimmer (Beam Dynamics, Model 1). The QMS was installed in the detection stage. In addition to the UHV technique, the detection sensitivity was improved by using a pulsed molecular-beam sampling method and digital counting electronics.

Preparation of Ice Films. The ice film was prepared by passing helium into a distilled water bubbler at 20.0 ± 0.1 °C. The helium−water vapor mixture was then admitted into the low-temperature flow reactor by a sliding injector, which was moved out at a constant speed during the course of the ice deposition. The ice film length was measured both just after the deposition and several minutes later. The latter length was shorter because the ice film evaporated and recondensed in the flow tube and we used this length to calculate the ice film thickness. The typical ice film length was 15 cm. The average thickness of the ice film was calculated by using the geometric area of the flow tube, the mass of ice deposited on the wall, and the bulk density of the vapor-deposited ice (0.63 g/cm^3).[23,24]

HBr−He and HBr−HCl−He Mixtures and Uptake Measurements. HBr−He mixtures were prepared by mixing HBr (Matheson, 99.8%) and helium (MG, Scientific grade 99.9999%) in a glass manifold, which had been previously evacuated to 2×10^{-6} Torr. The typical HBr-to-helium mixing ratio was $10^{-4}-10^{-5}$. The amount of HBr along with additional helium carrier gas introduced into the flow reactor was monitored with Monel flow meters (Teledyne-Hastings). The flow rate of the carrier gas was in great excess so that a small variation of HBr flow would not affect the total pressure. Before the uptake experiment, the HBr mixture was admitted into the reactor without contact with the ice film, the measured HBr signal being proportional to the concentration of HBr admitted into the flow tube. The HBr signal from a known concentration was used as a calibration standard for the HBr signal in the measurement. The HBr flow was then redirected to be in contact with the ice film for the uptake experiment. The loss of HBr onto the ice film was measured by the QMS at $m/e^- = 80$ and is shown in Figure 1 for a typical experiment. The total amount of HBr loss into the ice film just before the desorption (see Figure 1) is defined as the uptake of HBr on ice films. The desorption feature was observed in nearly all experiments conducted. In many experiments, the ice vapor pressure was measured simultaneously during the uptake experiment. The ice vapor signal, $m/e^- = 18$, was calibrated against a pure ice film at the constant temperature (188 K) with the presence of the helium carrier gas at the beginning of the experiment.

The HBr−HCl mixture was prepared by mixing pure HBr and HCl (Matheson semiconductor, 99.999%) gases at different pressures in the glass manifold, which was already evacuated to 10^{-6} Torr. The amount of both HBr and HCl before the mixing was calibrated at STP. The mixture was further diluted with helium in the glass manifold. To minimize the error in the pressure measurements for HBr and HCl gases, we kept the HCl-to-HBr mixing ratio in the range of 1−20.

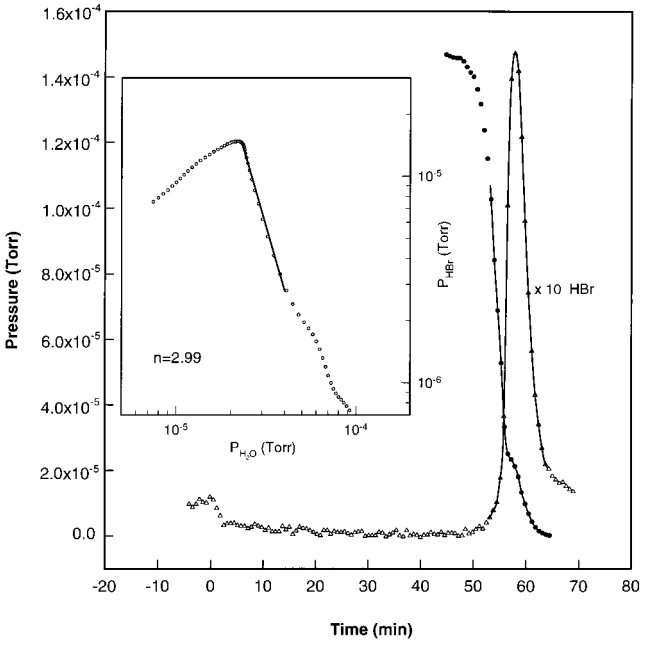

Figure 1. Plot of HBr (△) and water vapor (●) pressures versus the uptake time at 188 K and $P_{HBr} = 1.0 \times 10^{-6}$ Torr. The uptake experiment started at time $t = 0$, and a HBr desorption was observed at $t \sim 57.5$ min. The inset shows the plot of log P_{HBr} vs log P_{H_2O} during the desorption event in the uptake experiment. Both HBr and water pressures (counts) were measured and then interpolated on the *same* experimental time. The slope of the plot is equal to $-n$, the number of water molecules in an HBr hydrate, as described in the text.

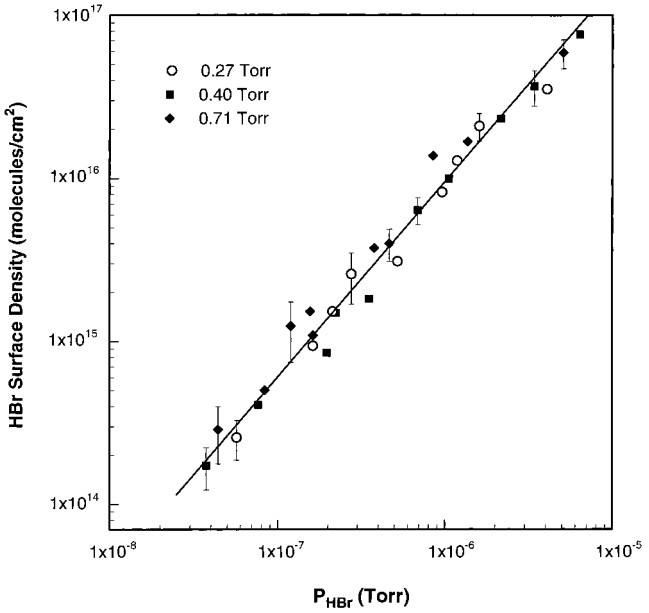

Figure 2. Plot of HBr uptake on ice films at 188 K as a function of the total pressures in the flow reactor and partial HBr pressures. The different symbols in the figure represent different total pressures. ○ is at 0.270 ± 0.008 Torr, ■ is at 0.406 ± 0.009 Torr, and ◆ is at 0.708 ± 0.009 Torr. The plot shows that there was no significant difference in the HBr uptake among these total pressures in the reactor. The solid line is the curve-fitting result as described in the text.

III. Results

HBr Uptake on a Water−Ice Film. HBr uptake as a function of total pressures is shown in Figure 2 and Table 1 with the detailed experimental conditions. In this figure, the uptake amount based on the geometric surface area is plotted versus the HBr partial pressures and total pressures. The different symbols in the figure show different total pressures in the flow reactor. A set of data with the total pressure of 0.4 Torr from our previous study[17] is also included in this figure. The results show that the uptake increased as partial HBr pressures increased. The uptake was independent of the total pressures within the pressure range that we studied. This indicates that a steady-state equilibrium is established between HBr and ice in the flow reactor. The solid line is fitted to[17,25,26]

$$P_{\mathrm{HBr}} = \mathrm{K}\theta^{f} \tag{4}$$

where P_{HBr} is the HBr partial pressure and θ is the HBr surface density on ice. We obtained $f = 0.83 \pm 0.05$ and $\mathrm{K} = 5.1 \pm 4.7 \times 10^{-20}$ from the least-squares fit. The fitted f value is in excellent agreement with our previous publication 0.80 ± 0.06.[17]

The HBr isotherm desorption amount is also listed in Table 1. The desorption amount was usually equal to the uptake amount. However, the desorption amount was lower than the uptake amount at $P_{\mathrm{HBr}} < 3 \times 10^{-7}$ Torr. The likely cause is that the desorption event was relatively rapid and we could catch only a few data points. This caused an error in computing the desorption amount.

HBr Hydrates. A HBr desorption peak was observed toward the end of the uptake experiment. This is shown as the triangles in Figure 1. We attributed this to the formation of a hydrate of hydrogen bromide on the ice film. A hydrate would be formed near the end of the uptake experiment if (1) the amount of HBr taken up by the ice surface could satisfy the stoichiometric requirement of the hydrate on the near-ice-surface layer, and (2) water vapor was driven away by adding HBr onto ice film surface. Providing that a steady-state equilibrium was established among the hydrate, HBr, and H_2O vapor pressures in the flow reactor, the following expression would be valid:

$$K' = P_{\mathrm{HBr}} \cdot P^{n}_{\mathrm{H_2O}} \tag{5}$$

where K' is the equilibrium constant, P_{HBr} and $P_{\mathrm{H_2O}}$ are the partial pressures of HBr and H_2O, respectively, and n is the number of water molecules in the hydrate. Both P_{HBr} and $P_{\mathrm{H_2O}}$ were measured sequentially by the QMS and are shown in Figure 1 by the solid circles and open triangles for the H_2O vapor pressure and HBr pressure, respectively. The time difference between the measured HBr signal versus H_2O signal was 1−3 s. The cubic spline method was used to interpolate these signals into the same time frame. They are shown as the solid lines in Figure 1 and open circles in the inserted figure. These interpolated HBr and H_2O pressures were used in eq 5 to determine the n value. The n value was then determined from the slope of a plot of log P_{HBr} versus log $P_{\mathrm{H_2O}}$ ($\log P_{\mathrm{HBr}} = -n \log P_{\mathrm{H_2O}} + \log K'$). Since both HBr and H_2O pressures were determined at exactly the *same time*, a dynamic steady-state equilibrium among vapor pressures of HBr, H_2O, and the solid hydrate was expected at any time during the desorption. The typical fitting is shown as a solid line in the insert of Figure 1. The average n values are listed in Table 2 under various experimental conditions. The numbers in the parentheses in Table 2 indicate the number of experiments used to calculate the mean n value. The results show that hydrobromic acid trihydrate was formed in most experiments and sometimes hydrobromic acid dihydrate was also formed. It is very important to point out that the n values are either 2 or 3 for about 50 experiments. Further evidence supporting HBr hydrate formation on ice films includes the phase diagram of the HBr−ice system.

HBr−Ice Phase Diagram. *Vapor Pressures of HBr and H_2O.* Little is known about the phase diagram of HBr−ice at temperatures below 200 K in terms of partial HBr and water vapor pressures.[27] The HBr−ice phase diagram was constructed to understand the thermodynamic properties of hydrates. The known thermodynamic properties of the HBr−H_2O system are HBr vapor−liquid equilibrium data at 20−55 °C,[28,29] the freezing points of the hydrate,[27] and ΔH of HBr·2H_2O at 258 K.[28] The partial HBr and water vapor pressures above the solution were calculated at their freezing points using a thermodynamic model.[30] The heat of sublimation of hydrates and the heat capacity of the hydrates were also computed to construct the phase diagram from thermodynamic considerations.

On the basis of a thermodynamic solution model developed by Carslow et al.,[30] the partial pressure of HBr can be calculated by

$$P_{\mathrm{HBr}} = \frac{f_{\pm}^{2} x_{\mathrm{H^+}} x_{\mathrm{Br^-}}}{{}^{x}K_{\mathrm{H}}} \tag{6}$$

where $f_{\pm}$ is the mean activity coefficient of two HBr ions, $x_{\mathrm{H^+}} = n_{\mathrm{H^+}}/(n_{\mathrm{H^+}} + n_{\mathrm{Br^-}} + n_{\mathrm{H_2O}})$ is the mole fraction of H^+ ion, $x_{\mathrm{Br^-}} = n_{\mathrm{Br^-}}/(n_{\mathrm{H^+}} + n_{\mathrm{Br^-}} + n_{\mathrm{H_2O}})$ is the mole fraction of Br^- ion, and ${}^{x}K_{\mathrm{H}}$ is the Henry's law constant on a mole fraction basis. Carslaw et al. parametrized expressions of $f_{\pm}$ and ${}^{x}K_{\mathrm{H}}$ for HBr solutions at 190−330 K. The calculated partial HBr pressure, P_{HBr}, as a function of temperatures (including at the freezing points) and compositions is shown Figure 3a. P_{HBr} at the freezing

TABLE 1: Uptake of HBr on Ice Films as a Function of Total Pressures and HBr Partial Pressures

P_{HBr} (Torr)	P_{total} (Torr)	temperature (K)	flow speed (cm/s)	uptake (molec/cm^2)	desorption (molec/cm^2)
4.08×10^{-6}	0.265	188.8	3.57×10^3	$(3.5 \pm 1.1) \times 10^{16}$	$(3.8 \pm 1.0) \times 10^{16}$
1.62×10^{-6}	0.271	187.5	3.57×10^3	$(2.1 \pm 0.4) \times 10^{16}$	$(2.2 \pm 0.6) \times 10^{16}$
1.19×10^{-6}	0.253	186.6	3.50×10^3	$(1.3 \pm 0.4) \times 10^{16}$	$(1.2 \pm 0.9) \times 10^{15}$
9.65×10^{-7}	0.270	186.8	3.51×10^3	$(8.3 \pm 1.7) \times 10^{15}$	$(6.3 \pm 1.4) \times 10^{15}$
5.23×10^{-7}	0.286	188.1	3.62×10^3	$(3.1 \pm 1.2) \times 10^{15}$	$(2.2 \pm 1.1) \times 10^{15}$
2.77×10^{-7}	0.275	187.2	3.61×10^3	$(2.6 \pm 0.9) \times 10^{15}$	$(1.8 \pm 0.8) \times 10^{15}$
2.14×10^{-7}	0.269	187.2	3.58×10^3	$(1.5 \pm 0.6) \times 10^{15}$	$(5.5 \pm 1.8) \times 10^{14}$
1.63×10^{-7}	0.269	188.8	3.60×10^3	$(9.4 \pm 3.2) \times 10^{14}$	$(3.8 \pm 1.6) \times 10^{14}$
5.69×10^{-8}	0.269	188.4	3.54×10^3	$(2.6 \pm 0.7) \times 10^{14}$	
5.10×10^{-6}	0.695	188.0	1.36×10^3	$(5.9 \pm 1.2) \times 10^{16}$	
1.37×10^{-6}	0.706	188.0	1.34×10^3	$(1.7 \pm 0.5) \times 10^{16}$	$(1.7 \pm 0.6) \times 10^{16}$
8.54×10^{-7}	0.720	188.3	1.40×10^3	$(1.4 \pm 0.6) \times 10^{16}$	$(1.4 \pm 0.6) \times 10^{16}$
4.67×10^{-7}	0.712	189.4	1.37×10^3	$(4.0 \pm 0.9) \times 10^{15}$	$(2.7 \pm 1.0) \times 10^{15}$
3.80×10^{-7}	0.695	188.9	1.41×10^3	$(3.7 \pm 0.9) \times 10^{15}$	$(2.3 \pm 1.2) \times 10^{15}$
1.63×10^{-7}	0.716	187.9	1.44×10^3	$(1.1 \pm 0.4) \times 10^{15}$	$(5.9 \pm 1.4) \times 10^{14}$
1.57×10^{-7}	0.706	188.8	1.50×10^3	$(1.5 \pm 0.5) \times 10^{15}$	$(1.5 \pm 0.4) \times 10^{15}$
1.20×10^{-7}	0.719	187.9	1.44×10^3	$(1.2 \pm 0.5) \times 10^{15}$	$(4.5 \pm 3.2) \times 10^{13}$
8.43×10^{-8}	0.705	188.0	1.47×10^3	$(5.0 \pm 1.7) \times 10^{15}$	$(3.9 \pm 2.0) \times 10^{13}$
4.42×10^{-8}	0.711	189.0	1.35×10^3	$(2.9 \pm 1.1) \times 10^{15}$	

TABLE 2: Determined Number of Water Molecules in the Hydrates at Different Temperatures and HBr Partial Pressures[a]

P_{HBr} (Torr)	T (K)		T (K)
	188.3 ± 0.4		195.1 ± 0.1
$(3.07 \pm 0.04) \times 10^{-6}$	2.97 ± 0.10 (9)	2.00 ± 0.04 (2)	1.96 ± 0.09 (16)
$(1.07 \pm 0.03) \times 10^{-6}$	3.04 ± 0.06 (5)	2.00 ± 0.01 (2)	1.98 ± 0.01 (2)
$(5.04 \pm 0.10) \times 10^{-7}$	2.95 ± 0.07 (13)		
mean n value	2.99	2.00	1.97

[a] The numbers in parentheses indicate the number of measurements conducted.

points can also be extrapolated by the Clausius−Clapeyron equation using partial HBr pressure data at 293−328 K. The extrapolated results, as the diamond symbol, are also shown in Figure 3a. Considering the errors and uncertainty of the methods, the partial pressures of HBr calculated by two methods are in reasonable agreement at the freezing points. The water vapor pressure was calculated by

$$P_{H_2O} = a_1 P^o_{H_2O} \tag{7}$$

where a_1 is the activity of the water and $P^o_{H_2O}$ is the saturation water vapor pressure. The water vapor pressure calculated from eq 7 is shown in Figure 3b. We also tabulated all the parameters used in eqs 6 and 7 along with both P_{HBr} and P_{H_2O} at their freezing points in Table 3.

ΔH of Hydrates. The coexistence line between two solid hydrates can be constructed by using the heat of sublimation of HBr·nH$_2$O and HBr·(n + 1)H$_2$O, where n = 2, 3, or 4, at the equilibrium temperature. The heat of sublimation, ΔH_{subl}, of HBr·2H$_2$O was calculated from the heat of formation of HBr·2H$_2$O, −688 kJ/mol,[28] at 258 K.

$$HBr\cdot 2H_2O(s) \overset{\Delta H_{subl}}{\rightleftharpoons} HBr(g) + 2H_2O(g) \tag{8}$$

$$\Delta H_{subl} = \Delta H^{HBr}_f + 2\Delta H^{H_2O}_f - \Delta H^{HBr\cdot 2H_2O}_f \tag{9}$$

ΔH^i_f can be calculated from $\Delta H^{o_i}_f + \int_{T_o}^{T} C_{p_i} dT$, where i represents the individual species, C_p is the heat capacity, and ΔH^o_f is the standard heat of formation. Both ΔH^{HBr}_f and $\Delta H^{H_2O}_f$ can be calculated using the temperature-dependent heat capacity[31,32] and heat of formation.[31] The heat capacity of HBr·2H$_2$O can be estimated using the Debye and Einstein theories.[33] HBr·2H$_2$O is a molecular crystal with an ionic structure. The heat capacity of the crystal has contributions from both lattice vibrations (Debye mode) of the ions and internal molecular vibrations (Einstein mode) of $H_5O_2^+$. This can be written as

$$C_v(\text{lattice}) = \sum_{i=1}^{\text{ions}} \frac{9R}{\left(\frac{\Theta_D}{T}\right)^3} \int_0^{\Theta_D/T} \frac{u_i^4 e^{u_i}}{(e^{u_i} - 1)^2} du_i \tag{10}$$

$$C_v(\text{internal}) = R \sum_{i=1}^{\text{ions}} \sum_{j=1}^{3n-6} \frac{x_{i,j}^2 e^{x_{i,j}}}{(e^{x_{i,j}} - 1)^2} \tag{11}$$

$$C_p \approx C_v = C_v(\text{lattice}) + C_v(\text{internal}) \tag{12}$$

where R is the universal gas constant and $u = h\nu/kT$. Θ_D is the Debye temperature of HBr·2H$_2$O and is determined from the highest phonon (lattice) vibrational frequency (∼200 cm^{-1}).[19] In eq 10, the summation was carried over to both cation and anion groups in the hydrate. The second summation in eq 11 was carried over to the 3n−6 vibrational modes within an ionic group and the other was summed over all ionic groups. $x_j = h\nu_j/kT$ where ν_j is a molecular vibrational frequency of the ionic group. We used all known IR bands[19] to calculate C_v; however, that did not include all 3n−6 modes. We assumed that the non-IR active modes had similar contributions to C_v as the IR parts, so to approximate, we used C_v(internal) ≈ 2C_v(IR modes). The calculated $C_p \approx 2C_v$(IR modes)+C_v(lattice) and ΔH_{subl} at different temperatures are listed in Table 4. The temperature-dependent heat capacity can be written as $C_p \approx C_v = 14.715 + 0.2723T - 2.853 \times 10^{-4}T^2$ (J/mol·K) where T = 258−180 K. A similar approach has been successfully applied to calculate the heat capacity of solid benzene[34] and ice.[35] We also used the same method to estimate the heat capacity of solids HNO$_3$·nH$_2$O, n = 1, 2, 3. The difference between the calculated heat capacity and experimental values was less than 1R.[36] These results clearly indicate that the calculated heat capacity of solid hydrates agrees reasonably well with the experimental data.

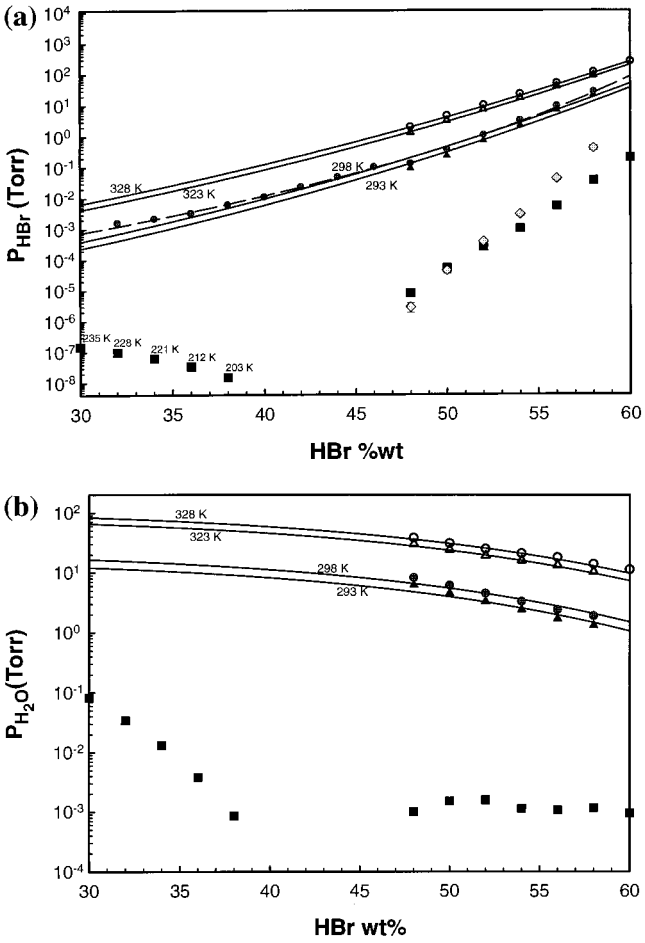

Figure 3. (a) Plot of partial HBr pressures over the solution at different temperatures and compositions. Both the solid lines and squares are model predictions. The dashed line is the least-squares fit of the data (●) from ref 28. Diamond symbols are extrapolated data at the freezing pointed based on the Clausius−Clapeyron equation. The difference between two calculation methods is a way to reflect the absolute uncertainty. (b) Plot of H_2O vapor pressure as a function of composition and temperature. The squares were calculated vapor pressures at the freezing points. Also see Table 3 for details.

TABLE 3: Partial Pressures of HBr and H_2O at Their Freezing Points

HBr wt %	T_z (K)	${}^xK_H$ (atm^{-1})	$f_\pm$	P_{HBr}(Torr)	a_{H_2O}	P_{H_2O}(Torr)
30.0	235.3	1.2593×10^9	6.1693	1.47×10^{-7}	0.6708	8.22×10^{-2}
32.0	228.2	3.8633×10^9	8.2044	9.93×10^{-8}	0.6245	3.42×10^{-2}
34.0	220.7	1.3358×10^{10}	11.2271	6.23×10^{-8}	0.5742	1.31×10^{-2}
36.0	212.2	5.7653×10^{10}	15.9155	3.35×10^{-8}	0.5197	3.81×10^{-3}
38.0	202.6	3.2306×10^{11}	23.5631	1.50×10^{-8}	0.4610	8.49×10^{-4}
48.0	209.5	9.3469×10^{10}	212.478	7.78×10^{-6}	0.1954	9.98×10^{-4}
50.0	214.2	4.0611×10^{10}	341.569	5.18×10^{-5}	0.1545	1.49×10^{-3}
52.0	216.6	2.6673×10^{10}	582.573	2.56×10^{-4}	0.1169	1.57×10^{-3}
54.0	216.8	2.6084×10^{10}	1078.69	9.99×10^{-4}	0.0835	1.13×10^{-3}
56.0	219.1	1.7425×10^{10}	1954.56	5.45×10^{-3}	0.0581	1.07×10^{-3}
58.0	223.1	8.9606×10^9	3436.60	3.63×10^{-2}	0.0395	1.16×10^{-3}
60.0	224.9	6.6488×10^9	6610.94	2.00×10^{-1}	0.0248	9.46×10^{-4}

Hisham and Benson[37] showed that the heat of formation, ΔH_f, of solid hydrates can be quantitatively correlated by a two-parameter equation

$$\Delta H_f(y_{m+n}) - \Delta H_f(x_m) = bn^\alpha \qquad (13)$$

where α and b are proportionality constants and α is close to unity. The quantities m and $m + n$ are the number of water molecules in a hydrate. We apply this equation to calculate

TABLE 4: Calculated Heat Capacity of $HBr\cdot 2H_2O$ and Heat of Sublimation of Hydrates at Different Temperatures

T (K)	$C_v(HBr\cdot 2H_2O)$ (J/mol K)	$HBr\cdot 2H_2O^a$ (kJ/mol)	$HBr\cdot 3H_2O^a$ (kJ/mol)	$HBr\cdot 4H_2O^a$ (kJ/mol)
217.0	60.4	163.0	219.6	276.4
213.0	59.8	162.8	219.5	276.2
203.0	58.2	162.5	219.2	275.9
193.0	56.6	162.1	218.8	275.5
183.0	55.0	161.7	218.4	275.1

[a] Heat of sublimation ΔH_{subl}. See text for details.

TABLE 5: Determination of b' Parameter in eq 14

species	$\Delta H_{subl}{}^a$ (kJ/mol)	$\Delta H(y_{m+n}) - \Delta H(x_m)$ (kJ/mol)	b' (kJ/mol)
$HCl\cdot 6H_2O$	371.4	164.2	54.7
$HCl\cdot 3H_2O$	207.2		
$HNO_3\cdot 3H_2O$	232.2	56.9	56.9
$HNO_3\cdot 2H_2O$	175.3	54.9	54.9
$HNO_3\cdot H_2O$	120.4		
$H_2SO_4\cdot 6^1/_2H_2O$	482.0	132.7	53.1
$H_2SO_4\cdot 4H_2O$	349.3	55.6	55.6
$H_2SO_4\cdot 3H_2O$	293.7	58.7	58.7
$H_2SO_4\cdot 2H_2O$	235.0	62.8	62.8
$H_2SO_4\cdot H_2O$	172.2		
mean			56.7 ± 3.2

[a] After ref 36.

ΔH_{subl}, because the difference between ΔH_f and ΔH_{subl} of two hydrates is a constant ($n\Delta H_f^{H_2O}$). Thus, eq 13 can be rewritten as

$$\Delta H_{subl}(y_{m+n}) - \Delta H_{subl}(x_m) = b'n^\alpha \approx b'n \qquad (14)$$

The proportionality coefficient b' can be determined from a set of hydrates. Values of b' are in Table 5 for a series of solid hydrates important to polar atmospheric chemistry. Using the determined mean b' value, 56.7 ± 3.2 kJ/mol, and $\Delta H_{subl}^{HBr\cdot 2H_2O}$, we estimated $\Delta H_{subl}^{HBr\cdot 3H_2O}$ and $\Delta H_{subl}^{HBr\cdot 4H_2O}$ from eq 14. The results are listed in Table 4.

Phase Diagram. Using the partial pressures of HBr and H_2O, the freezing points T_z, and ΔH_{subl} in Tables 3 and 4, we determined the coexistence lines of the $HBr\cdot 2H_2O$, $HBr\cdot 3H_2O$, and $HBr\cdot 4H_2O$ phases. The coexistence lines in the phase diagram can be expressed as[36]

$$\frac{d \ln P_{HBr}}{d(1/T)} = \frac{m\Delta H_{subl}(y_{m+n}) - (m+n)\Delta H_{subl}(x_m)}{nR} \qquad (15a)$$

$$\frac{d \ln P_{H_2O}}{d(1/T)} = -\frac{\Delta H_{subl}(y_{m+n}) - \Delta H_{subl}(x_m)}{nR} \qquad (15b)$$

The calculated coexistence lines are shown as the solid lines in Figure 4. At the triple point of $HBr\cdot 2H_2O$, $HBr\cdot H_2O$, and the liquid phase, the parametrized thermodynamic model[30] predicts that the HBr partial pressure will be about 5-fold higher than the literature value.[28] The solid coexistence line (cyan) between $HBr\cdot 2H_2O$ and $HBr\cdot H_2O$ was calculated from the intercept of the isotherms and the equilibrium HBr vapor pressure. The HBr vapor pressure was computed using eq 15a. We assumed that P_{HBr} at the triple point was equal to the total vapor pressure $P_{total} = 1700$ Torr.[28] The water vapor pressure at the triple point was estimated to be about 3×10^{-3} Torr, so this assumption was well justified. Isotherms at every two-degree interval are also plotted in the figure. The slope, $-n$, of the isotherm is −2.0, −3.2, and −4.0 in the $HBr\cdot 2H_2O$, $HBr\cdot 3H_2O$, and $HBr\cdot 4H_2O$ phase, respectively. The n value is a good

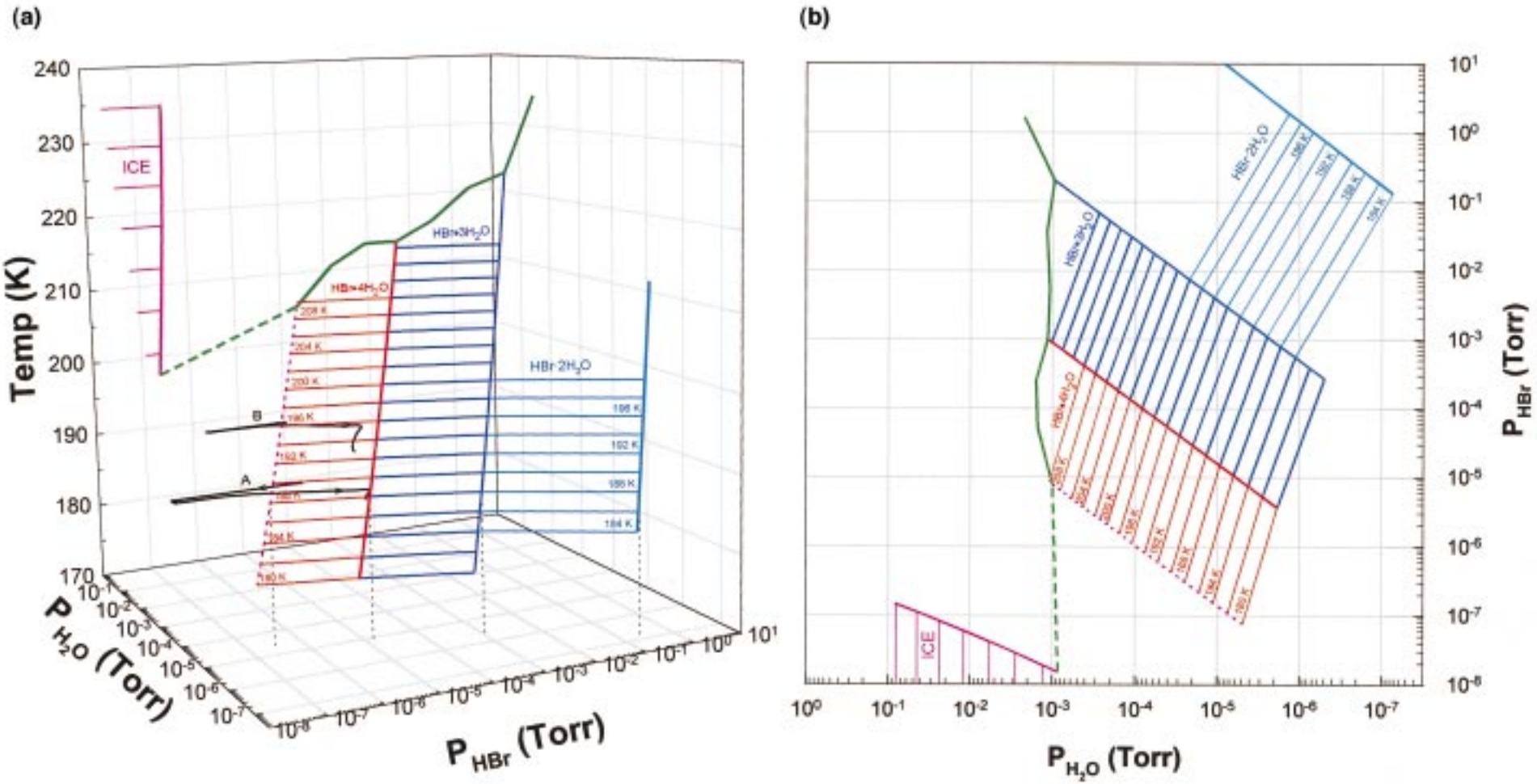

Figure 4. Phase diagram of the HBr and ice system. The composition and freezing points determined the phases of hydrates. The coexistence lines between the solid hydrates and isotherms were computed using eqs 15 a and b. (a) Line A is a trace of the HBr uptake on ice at 188 K with initial $P_{HBr} = 3.0 \times 10^{-6}$ Torr; the uptake starts from pure ice and finally forms $HBr{\cdot}3H_2O$ which is indicated by the slope of -3 in the plot. Line B is at 195 K and indicates formation of $HBr{\cdot}2H_2O$. The drop lines indicate P_{HBr} and P_{H_2O} at 188 K. (b) Top perspective of the phase diagram.

indication of thermodynamic consistency and, perhaps, represents a degree of the calculation accuracy. When one views this 3-D phase diagram (Figure 4a) from the front perspective, the phases in front of these colored planes belong to the stable thermodynamic region. We also provide a top view of the phase diagram in Figure 4b.

The uncertainty in the phase diagram can be estimated from several sources. Vapor pressures of HBr and water, the heat of sublimation, and the freezing envelope are three critical components. The average deviation for estimating the heat of formation is less than 1 kcal/mol using eq 13.[37] The standard deviation of the b' value in eq 14 is 3.2 kJ/mol for a series of low-temperature solid hydrates. Assuming that the same trend applies to HBr·nH$_2$O, the estimated error for ΔH_{subl} is less than 4 kJ/mol. Note that the uncertainty for the heat of sublimation is larger than that of the heat capacity of the solid hydrate. The uncertainty of P_{HBr} and $P_{\mathrm{H_2O}}$ at the freezing points and the freezing point itself seem to have the largest impact on the profile of the phase diagram. The absolute error of the partial pressures is estimated to be a factor of 2 to 5, on the basis of Figure 3.

HBr partial pressures and ice vapor pressures monitored during the uptake process were plotted in the 188 and 195 K plane of Figure 4a as line A and line B, respectively. Line A shows that the uptake starts from pure water-ice (before the uptake experiment) and then eventually transfers into the HBr·3H$_2$O state as indicated by arrows. The formation of the trihydrate is indicated by the slope of line A, as it approaches the HBr·3H$_2$O phase region, to be −3. The final state of the desorption in line A falls directly into the stable HBr·3H$_2$O region, and the line is in the front of the phase plane. This unique evidence shows that a stable HBr·3H$_2$O was formed toward the end of the uptake experiment. The continuous evacuation in the flow tube forced line A to shift out of the HBr·3H$_2$O phase again. Line A also indicates that a meta-stable HBr·3H$_2$O was formed in the tetrahydrate phase region during the uptake. In some experiments, a meta-stable HBr·3H$_2$O hydrate is the only product; the stable HBr·3H$_2$O hydrate was never formed. There were cases in which meta-stable HBr·2H$_2$O was formed in the stable hydrobromic acid tetrahydrate region, and this is indicated by the slope of the partial HBr and H$_2$O pressure curve of −2 (line B in Figure 4a). This indicates that HBr·2H$_2$O was not formed directly from the gas phase; it is rather formed near the ice surface through the transformation of adsorbed HBr. A similar situation was found in the HNO$_3$−ice phase diagram where meta-stable HNO$_3$·H$_2$O and HNO$_3$·2H$_2$O were formed in HNO$_3$·3H$_2$O phase region[38] and HCl−ice phase diagram.[36] HBr·3H$_2$O is a thermodynamically stable compound, more so than HBr·2H$_2$O. HBr·2H$_2$O would probably transform into HBr·3H$_2$O. However, at the point of desorption, the vapor-phase species were constantly being evacuated by the pump in the flow reactor. The residence time of newly formed hydrates in the flow tube was a few minutes (cf. Figure 1, ∼55−58 min). This time scale may not be long enough to have a phase transformation completed from HBr·2H$_2$O into HBr·3H$_2$O. However, the composition in the gas phase was already across a phase boundary. This is a possible reason meta-stable HBr·2H$_2$O was observed in some experiments.

Effect of the Film Thickness on HBr Uptake. The HBr uptake on ice was measured as a function of ice film thickness at different partial HBr pressures ranging from 1.0×10^{-6} to 2.1×10^{-7} Torr. The film thickness varied from 0.45 to 16.7 μm. The results are shown in Figure 5 as the logarithm of the uptake versus the film thickness at different partial HBr pressures. The uptake increased dramatically as the film got thicker in the region 0.5−5 μm. The uptake increased by about a factor of 15 as the ice film thickness varied from 1 to 10 μm. We believe that there are a few factors contributing to this, the most significant being ice film surface morphology and the dynamic nature of ice.[23,39]

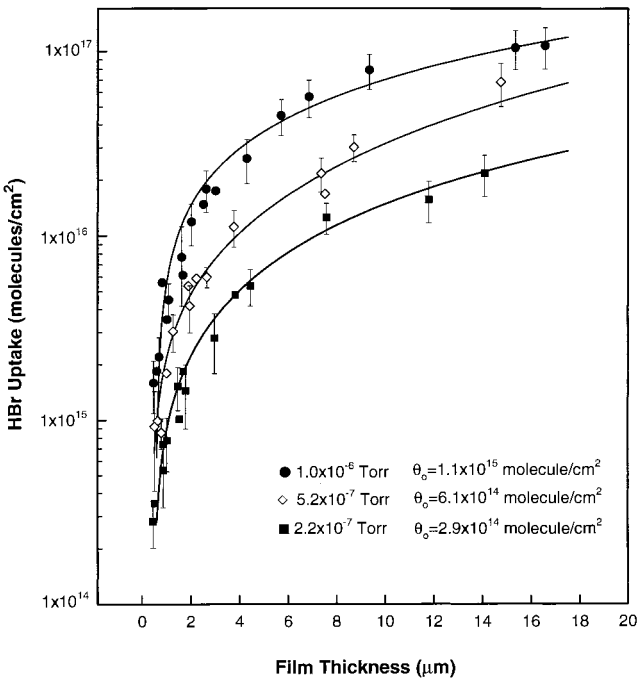

Figure 5. Plot of HBr uptake as a function of ice film thickness at different partial HBr pressures (● $1.02 \pm 0.03 \times 10^{-6}$ Torr, ◇ $5.15 \pm 0.30 \times 10^{-7}$ Torr, and ■ $2.19 \pm 0.30 \times 10^{-7}$ Torr) and 188 K. The solid lines are fitted into an ice micro-granule model as discussed in the text. The fitted "true" surface coverage θ_os are 1.1×10^{15}, 6.1×10^{14}, and 2.9×10^{14} molecules/cm^2 for $P_{\mathrm{HBr}} = 1.0 \times 10^{-6}$, 5.2×10^{-7}, and 2.2×10^{-7} Torr, respectively.

In this study, the ice film roughness originated from the water-vapor nucleation process on the glass reactor wall during vapor deposition and the recondensation of the ice vapor in the reactor. There are some differences in these two processes such as the saturation water−vapor ratio. As a first-order approximation, we modeled the ice film in terms of micrometer-sized ice granules stacked in layers.[40,41] The spherical ice granules were packed in an hexagonal structure layer by layer. The HBr uptake amount was proportional to the total surface area of the hexagonal-packed ice granules.[23,41] In the model calculation, the mean ice granule size was assumed to be similar to that determined from separate experiments under similar conditions;[24,41] thus the ice granule size was empirically correlated to the ice film thickness. Keyser et al.[24,41] determined that the mean ice granule size is about 0.5 μm for an ice film of 1 μm thickness, and is 1 μm for an ice film of 10 μm thickness.

The experimental results can be fitted into the micrometer-sized ice granule model with the above ice granule size distribution.[23,40,41]

$$\text{Uptake} = \theta_o \frac{\pi}{\sqrt{3}}\left(2N_L - 1 + \sqrt{\frac{3}{2}}\right) \qquad (16)$$

where θ_o is the "true" HBr surface coverage. N_L is the number of granule layers. A slightly different granule layer distribution expression as determined by Keyser et al.[41] was used in order

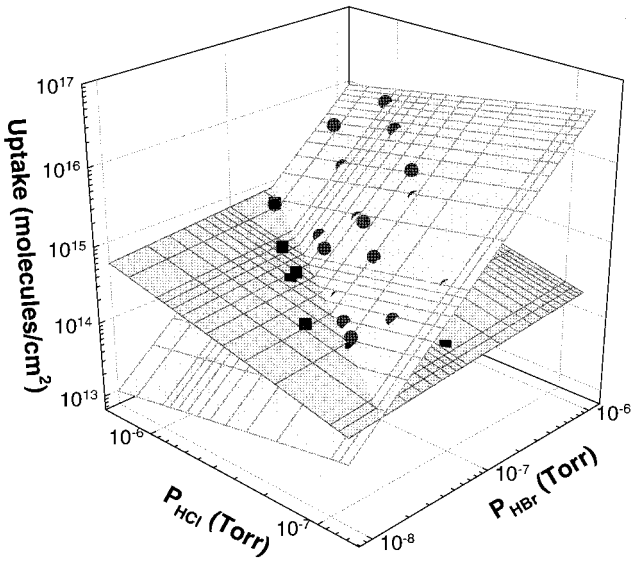

Figure 6. Plot of HBr (●) and HCl (■) co-uptake as a function of partial HBr and HCl pressures at 188 K. The planes through the data are the best fits. HBr uptake was affected by the presence of HCl on ice.

to cover all experimental thickness. The fitting results are shown in Figure 5 as the solid lines for three sets of experiments. The determined θ_o values are also shown in Figure 5. The error in fitting θ_o was very large because the HBr surface coverage converged rapidly as a function of the ice film thickness. The uncertainty factor in θ_o is about 2. θ_o is about 5−10-fold smaller than the measured surface density shown in Figure 2 at the same partial HBr pressure condition. The lower θ_o value indicates that some HBr molecules were adsorbed on the inner ice granule layer surfaces through a pore diffusion mechanism. The true HBr surface coverage, $\theta_o = 1.1 \times 10^{15}$ molecules/cm^2 at $P_{HBr} = 1.0 \times 10^{-6}$ Torr (see Figure 5), seems to indicate a "multilayer" adsorption. This analysis shows that the nature of the multilayer is not the HBr uptake onto the inner ice granule surface. It is rather the formation of hydrates near the ice granule surface layer as was discussed previously.

We can also fit θ_o as a function of partial HBr pressures in terms of eq 4. The f value obtained from this fitting is 0.89 ± 0.24. The large error came from the larger uncertainty of fitted θ_o. This f value is consistent with the $f = 0.83$ value obtained directly from fitting the experimental data.

Co-uptake of HBr and HCl on Ice. The experiments on the competitive co-uptake of HBr and HCl on ice were designed to elucidate the effect of the presence of HCl on the HBr uptake on ice and to test the relative strength of uptake. In these experiments, the HCl molecules reached saturation level quickly and the time needed to saturate with HBr molecules resembled the HBr uptake experiment as illustrated in Figure 1. Again, desorption of HBr toward the end of the co-uptake experiment was observed in all experiments. The changes in ice vapor pressures near the end of the uptake process also forced the HCl molecules to desorb. For HBr and HCl pressures ranging from about 1.0×10^{-6} to 2.8×10^{-8} Torr, the HBr + HCl co-uptake at 188 K and at a film thickness of 1.5 ± 0.3 μm is shown in Figure 6. Figure 6 is a 3-D logarithmic plot. The vertical axis is the uptake of either HBr or HCl at a given partial HBr and HCl pressure. Sometimes, it is difficult to read the uptake amount from the 3-D plot, but it provides a nice profile of the uptake as function of both P_{HBr} and P_{HCl}. We also provide the uptake amount along with the standard deviations and experimental conditions in Table 6. The two planes are the least-squares fit to the experimental data in the form of

$$\log \theta = f'_{HBr} \log P_{HBr} + f'_{HCl} \log P_{HCl} + K'' \qquad (17)$$

where θ is the surface density of either HBr or HCl. The fitted parameters f' and K'' are tabulated in Table 7. Figure 6 indicates that the HBr uptake increased with HBr partial pressures and decreased with HCl partial pressures. HCl uptake also increased with HCl partial pressures and slightly decreased with HBr partial pressures.

TABLE 6: Co-uptake of HBr and HCl on Ice[a]

P_{HBr} (Torr)	P_{HCl} (Torr)	T (K)	HBr uptake (molecules/cm^2)	HCl uptake (molecules/cm^2)
2.85×10^{-8}	2.80×10^{-7}	188.2	$(1.2 \pm 0.4) \times 10^{14}$	$(2.7 \pm 0.6) \times 10^{14}$
3.68×10^{-8}	1.84×10^{-7}	188.2	$(2.3 \pm 0.4) \times 10^{14}$	$(1.6 \pm 0.3) \times 10^{14}$
4.71×10^{-8}	2.39×10^{-7}	188.0	$(2.4 \pm 0.8) \times 10^{14}$	$(1.7 \pm 0.5) \times 10^{14}$
5.59×10^{-8}	5.49×10^{-7}	188.2	$(1.6 \pm 0.4) \times 10^{14}$	$(3.4 \pm 0.7) \times 10^{14}$
5.69×10^{-8}	5.13×10^{-7}	188.0	$(2.6 \pm 0.4) \times 10^{14}$	$(4.4 \pm 0.7) \times 10^{14}$
5.71×10^{-8}	1.44×10^{-7}	188.2	$(3.6 \pm 1.0) \times 10^{14}$	$(1.9 \pm 0.7) \times 10^{14}$
6.85×10^{-8}	3.32×10^{-7}	188.5	$(2.7 \pm 0.8) \times 10^{14}$	$(2.1 \pm 0.5) \times 10^{14}$
8.16×10^{-8}	8.02×10^{-7}	188.0	$(2.9 \pm 0.7) \times 10^{14}$	$(5.1 \pm 1.3) \times 10^{14}$
1.05×10^{-7}	1.08×10^{-7}	188.0	$(8.2 \pm 1.5) \times 10^{14}$	$(1.4 \pm 0.3) \times 10^{14}$
1.05×10^{-7}	5.29×10^{-7}	188.2	$(6.0 \pm 1.2) \times 10^{14}$	$(3.4 \pm 0.5) \times 10^{14}$
1.10×10^{-7}	9.95×10^{-7}	188.0	$(3.6 \pm 0.5) \times 10^{14}$	$(4.1 \pm 1.7) \times 10^{14}$
1.13×10^{-7}	2.85×10^{-7}	188.0	$(7.7 \pm 2.7) \times 10^{14}$	$(2.0 \pm 0.8) \times 10^{14}$
1.37×10^{-7}	6.76×10^{-7}	188.2	$(6.1 \pm 1.7) \times 10^{14}$	$(3.2 \pm 0.7) \times 10^{14}$
1.62×10^{-7}	1.46×10^{-6}	188.0	$(7.7 \pm 2.4) \times 10^{14}$	$(8.0 \pm 2.0) \times 10^{14}$
1.67×10^{-7}	4.21×10^{-7}	188.1	$(1.2 \pm 0.4) \times 10^{15}$	$(3.0 \pm 0.7) \times 10^{14}$
1.99×10^{-7}	5.07×10^{-7}	188.4	$(1.1 \pm 0.2) \times 10^{15}$	$(3.9 \pm 0.9) \times 10^{14}$
1.99×10^{-7}	9.84×10^{-7}	188.1	$(6.7 \pm 0.9) \times 10^{14}$	$(4.2 \pm 1.0) \times 10^{14}$
3.02×10^{-7}	3.11×10^{-7}	188.2	$(2.3 \pm 0.3) \times 10^{15}$	$(2.5 \pm 1.3) \times 10^{14}$
3.76×10^{-7}	3.73×10^{-7}	188.3	$(4.0 \pm 0.7) \times 10^{15}$	$(4.3 \pm 0.9) \times 10^{14}$
3.86×10^{-7}	9.82×10^{-7}	188.3	$(2.1 \pm 0.3) \times 10^{15}$	$(5.0 \pm 1.9) \times 10^{14}$
5.66×10^{-7}	1.44×10^{-6}	188.3	$(4.7 \pm 1.8) \times 10^{15}$	$(8.4 \pm 2.1) \times 10^{14}$
6.99×10^{-7}	6.94×10^{-7}	188.1	$(6.2 \pm 1.2) \times 10^{15}$	$(4.9 \pm 1.0) \times 10^{14}$
1.01×10^{-6}	1.00×10^{-6}	188.4	$(9.3 \pm 2.9) \times 10^{15}$	$(7.2 \pm 3.0) \times 10^{14}$

[a] The error ($\pm\sigma$) includes the HBr + HCl preparation, calibration, and measurement errors in every experiment.

The effect of HCl on HBr uptake can be explained as follows. Both HCl and HBr molecules compete to occupy available ice surface sites at nearly the same rate.[21] When a site is occupied by an HCl molecule, it may not be available to HBr. The more HCl molecules in the gas phase, the higher the HCl surface coverage. It ultimately decreases the HBr uptake and the formation of HBr hydrates. In addition, with the presence of HCl resulting in higher acidity on the ice film surface, the nature of HBr dissociation on ice may be modified. The large effect of HCl on the HBr uptake also comes from the fact that formation of hydrates involves four formula units per unit cell surface area (see below).

On the other hand, when HCl reaches the saturation coverage on the ice surface, perhaps less than half of total surface sites are occupied by both HCl and HBr molecules because HCl has a submonolayer coverage on ice under PSC conditions. There are sufficient "vacant" sites still available for both HBr and HCl, and ultimately the effect of HBr on the HCl uptake is smaller. The nature of HCl ionization over the ice surface is affected by the presence of HBr as well.

Discussion

HBr−Ice Phase Diagram. The general profile of the HBr−ice phase diagram is very similar to those for HCl−ice, HNO_3−ice, and H_2SO_4−ice at polar atmospheric temperatures.[42,36] Some differences lie in the hydrate stable regions. In the HNO_3−ice phase diagram, for example, the stable $HNO_3 \cdot 3H_2O$ phase exists in the concentration ranges from about 33 to 72 wt % in solution. As a result, the liquid−solid coexistence line varies widely with

TABLE 7: Comparison of the *f* Parameters in Different Experiments

		f'_{HBr}	f_{HBr}	f'_{HCl}	f_{HCl}	K'	remark
co-uptake	HBr	1.38 ± 0.05	0.72 ± 0.03	-0.39 ± 0.07		21.88 ± 0.4	this work
	HCl	0.14 ± 0.05		0.57 ± 0.07	1.8 ± 0.2	19.02 ± 0.4	this work
uptake	HBr		0.83 ± 0.05				this work
	HBr		0.80 ± 0.06				ref 17
	HCl				2.0 ± 0.1		this work
	HCl				1.8		ref 23

temperature. This is not the case for the $HBr \cdot 3H_2O$ phase, which exists in the concentration ranges from 54 to 60 wt % of the aqueous phase. The liquid−solid coexistence line varies slightly with the temperature. This basically reflects the nature of those hydrates at low temperature.

Figure 4a shows that there is a slight temperature discrepancy between the isotherms and experimental data (e.g., line A). Line A is about 2 K warmer than the isotherm at 188 K. This slight discrepancy may well be within the uncertainty of the measurements and vapor pressure calculations. There are two possible reasons for this. (i) The isotherms were calculated on the basis of the heat of sublimation of hydrates and both P_{HBr} and P_{H_2O} at the freezing points. Uncertainty exists on ΔH_{subl}, P_{HBr}, and P_{H_2O} as discussed previously and results in a temperature uncertainty estimated to be about 1−2 degrees. (ii) The thermocouples, which measured the ice film temperature, were placed on the outside wall of the glass flow reactor. The ice film was deposited on the inside glass wall and the "true" temperature of the ice film may have been about 1−2 degree warmer than measured. Therefore, the slight temperature discrepancy is within experimental uncertainty.

Hydrates. Molecular dynamic simulation of HCl on ice shows that HCl molecules are adsorbed on the ice surface and then ice growth incorporates the adsorbed HCl into the newly formed bilayer.[43] This leads to the dissociation of the HCl molecule near the ice surface. Similar processes may take place for HBr on ice. We expect that the adsorbed HBr molecules probably interact with many H_2O molecules in the initial uptake stage. Most likely, the incorporation of HBr into the "ice lattice" has to be in a specific configuration in order to form $HBr \cdot 3H_2O$. It is reasonable to assume that the hydrate formed over the ice film surface has the same structure as the $HBr \cdot 3H_2O$ single-crystal (we ignore any defects and surface effects). In the bulk structure,[20] one oxygen atom O(1) is surrounded by two oxygen atoms O(2) and two bromine atoms in approximately tetrahedral coordination separated by the distance of a hydrogen-bond, whereas the two other oxygen atoms O(2) have a pyramidal environment bonded to another bromine atom and neighboring oxygen atoms. This is illustrated in Figure 7. The O(2)····H··· ··O(2) hydrogen-bond length is shorter than a hydrogen bond between normal water molecules. This indicates the formation of the ionic form $H_5O_2^+$ where a proton is transferred from HBr.

The high uptake of HBr on ice can be explained in terms of the hydrate formation near the ice surface. Hydrates dramatically change the coordination number of bromine to H_2O. In an orthorhombic $HBr \cdot 3H_2O$ unit cell, there are 4 Br atoms per unit cell (see Figure 7). When HBr molecules adsorb on the ice surface, one (or more) layer of the orthorhombic $HBr \cdot 3H_2O$ crystal was then expected to form *above* the ice surface so that hydrate has the sufficient vapor pressure to be detected by the QMS in our experiments. If this were the case, four HBr molecules (assuming one unit-cell layer) would be taken up by ice *per hydrate unit-cell surface area*. Although this area is about twice the area of the ice basal plane,[44] it would provide a higher HBr uptake. Also there are four formula units of $HBr \cdot 2H_2O$ in a $HBr \cdot 2H_2O$ unit cell.[20] Both $HBr \cdot 2H_2O$ and $HBr \cdot 3H_2O$ share a common ionic group, i.e., $H_5O_2^+Br^-$, which shows a similar chemical behavior; a similar uptake is expected. Note the HBr uptake extends beyond the simple 2-D surface adsorption. However, substantial incorporation of HBr or bromide into bulk ice is unlikely to occur. There are a few reasons: HBr or bromide remaining on the ice surface would be lower the surface Gibbs free energy of the system;[45] the larger size of Br and lower ion mobility of Br^- result in a lower diffusion rate of HBr than HCl in ice;[17] the formation of the $HBr \cdot 3H_2O$ crystal inside the ice lattice results in a lattice-size mismatch. These facts suggest that HBr molecules predominantly remain near the ice surface in a form of hydrate in the experimental time scale.

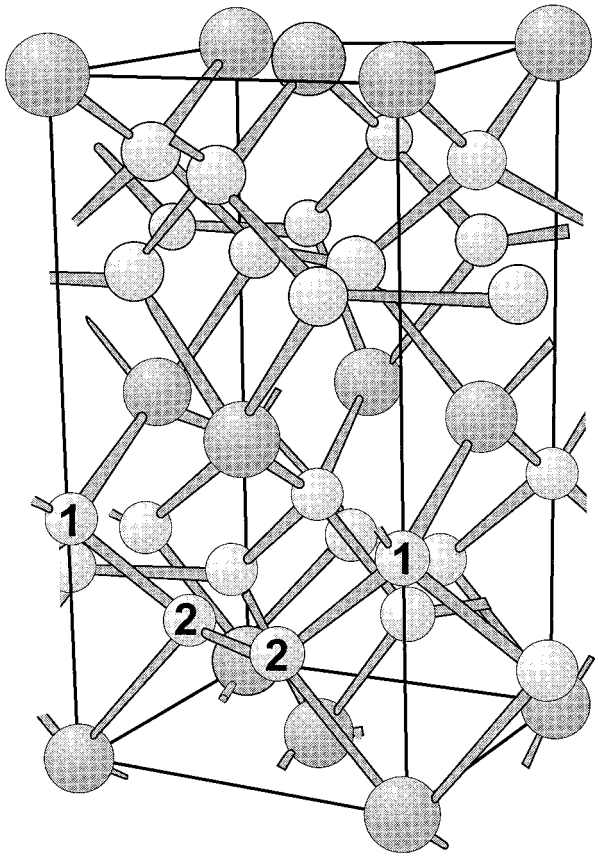

Figure 7. Crystal lattice structure of $HBr \cdot 3H_2O$, redrawn after ref 20. The large balls represent the bromine atoms and the small balls represent oxygen atoms. Oxygen atoms are in two different crystal sites as described in the text. Hydrogen atoms are not shown. The figure shows 4 Br atoms per unit cell. This hydrate is formed on the ice surface at 188 K.

One would logically expect that a stable $HBr \cdot 4H_2O$ hydrate could be formed under our experimental conditions (cf. Figure 4). However, this study showed that both $HBr \cdot 3H_2O$ and $HBr \cdot 2H_2O$ are formed at $P_{HBr} \sim 10^{-6}-10^{-7}$ Torr and 188 and 195 K (see Table 2). A phase diagram presenting vapor pressures as a function of temperature can be used to place constraints on the existence of various solid phases in the laboratory

experiments. The stability region of the phase diagram does not necessarily imply formation of a solid hydrate. Nucleation needs to take place first if a condensed phase (e.g., $HBr \cdot 4H_2O$) is to be formed from vapor or from a liquid or another solid phase. It is unlikely to form from the liquid phase in this study simply because the substrate is ice at 188 K. Under the flow tube conditions, the ice film is constantly evaporating and accommodating at the steady-state equilibrium. This behavior leads to some degrees of nonequilibrium. The net result is as follows: (1) It effectively changes the vapor−solid partitioning toward the end of the uptake experiment. Water molecules are preferentially removed faster than HBr molecules because of the higher vapor pressure. This is a limitation of the flow system in studying thermodynamic equilibrium properties; however, it will not affect the determination of hydrate composition because we used a dynamic measurement method. (2) The change of water vapor pressure near the desorption region, as with HBr, leads to a solid-phase transformation or across the coexistence lines. As already discussed, if the nuclei for the second phase do not form readily, the first phase persists into the stable region of the second phase until the first solid evaporates (desorption phenomena).[36] The meta-stable species of the second phase (e.g., $HBr \cdot 2H_2O$ or $HBr \cdot 3H_2O$) can be formed.

A long-term goal of this study is to understand the effect of the ionic nature of $H_5O_2^+Br^- \cdot H_2O$ or $H_5O_2^+Br^-$ hydrate on the heterogeneous reactions on ice surfaces such as reaction 3. Understanding the nature of the bonding between Br and ice (hydrate) is essential to reveal the reaction mechanism at a molecular level. For example, Hanson and Ravishankara noticed that the product BrCl in the $ClONO_2$ + HBr reaction on an ice film was not detected directly in the gas phase when HBr is in excess.[15] Also, we found that it is difficult to detect gas-phase BrCl in the HOCl + HBr reaction over the ice film,[46] while BrCl is detected in the gas phase for the reaction of HOBr + HCl.[16,47,48] This implies that the nature of the Br^-−H_2O surface bond may be different from that of Cl^-−ice. This is a first step toward understanding the reaction mechanism at the molecular level.

Comparison with Previous Studies. *HBr Uptake*. The HBr uptake amount is independent of total pressure in the flow reactor, thus the HBr uptake obtained from this study was identical to our previous study.[17] This result is in good agreement with the measurement of Hanson and Ravishankara.[15]

Abbatt[16] studied this system at higher partial HBr pressures (1.2×10^{-4} Torr) and temperatures (228 K). Under those experimental conditions, if the system is in perfect thermodynamic equilibrium condition, the final state of the uptake occurs in the liquid phase as illustrated in Figure 4b.

Co-uptake of HBr and HCl. The difference between the uptake of HBr or HCl on ice versus the competitive co-uptake of HBr + HCl on ice is shown in Figure 8. The HCl uptake on ice was nearly identical to the amount of the HBr + HCl co-uptake experiment as shown in Figure 8a. The measured HCl uptake amount in this study was in excellent agreement with previous publication.[23,49,50] The HBr uptake on ice was slightly higher than that of HBr in the HBr + HCl co-uptake experiment, when partial HCl pressure was about 10^{-6} Torr. The HBr uptake amount in the HBr + HCl co-uptake experiment was close to the HBr uptake on ice in a lower $P_{HCl} \sim 10^{-7}$ Torr region. These trends are shown in Figure 8b. One can also examine the f parameters, determined from eq 4 for the uptake experiment and eq 17 for the co-uptake experiment, to obtain similar conclusions, if f'_{HBr} and f'_{HCl} are considered to be two linear independent coefficients, i.e., these parameters represent either

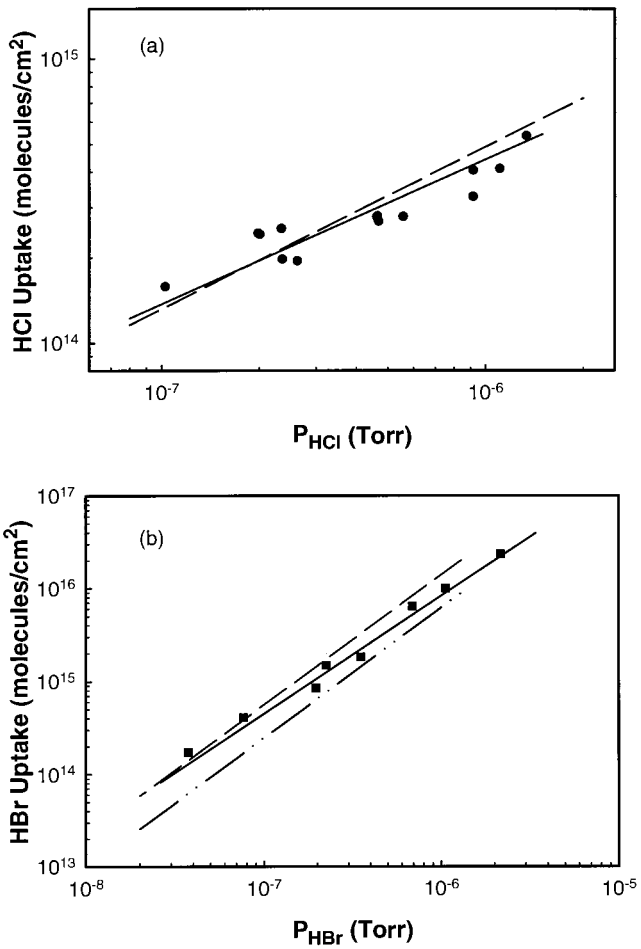

Figure 8. (a) Comparison of the HCl uptake (●) versus HCl co-uptake (dashed line) at 188 K. The dark solid line is the least-squares fit of the HCl uptake data and the dashed line was calculated from eq 17 with $P_{HBr} = 1 \times 10^{-7}$ Torr. (b) HBr (■) uptake versus HBr co-uptake on ice. Two dashed lines were computed for HBr co-uptake amounts at $P_{HCl} = 10^{-7}$ Torr (− −) and 10^{-6} Torr (− ·· −), respectively. The plot indicates that the HBr uptake is slightly higher than that of the co-uptake amount at lower P_{HCl} conditions.

HBr or HCl uptake behavior individually. We can treat $f = 1/f'$ approximately. These new parameters f_{HBr} and f_{HCl} are listed in Table 7. The nearly identical f values for both uptake and co-uptake experiments (columns f_{HBr} and f_{HCl} in Table 7) suggest the interaction between HCl and HBr is small compared with the interaction between HCl and ice or between HBr and ice. A small negative value in Table 7 implies that HBr uptake is in part inhibited by the presence of HCl on ice films. Also, a very small, 0.14, value indicates that the HCl uptake amount in the co-uptake experiment was scarcely influenced by the presence of HBr.

Atmospheric Application. Whether hydrobromic acid hydrates can be formed near the type II PSC surfaces is of interest to atmospheric chemists. The gas-phase HBr concentration is about 1.6−2 pptv in the middle latitude of the stratosphere.[51,52] In the polar region, the gas-phase HBr concentration is likely decreased by a factor of 10 or more with a source of HBr production absent and HBr uptake on PSCs.[11] This means the partial HBr pressure is on the order of 10^{-11} Torr or lower. This pressure is lower than our experimental conditions. Our experimental results cannot directly reflect the HBr heterogeneous uptake on type II PSCs; however, it is possible to comment on the thermodynamic state of HBr near the ice surface on the basis of the constructed HBr−ice phase. We replotted

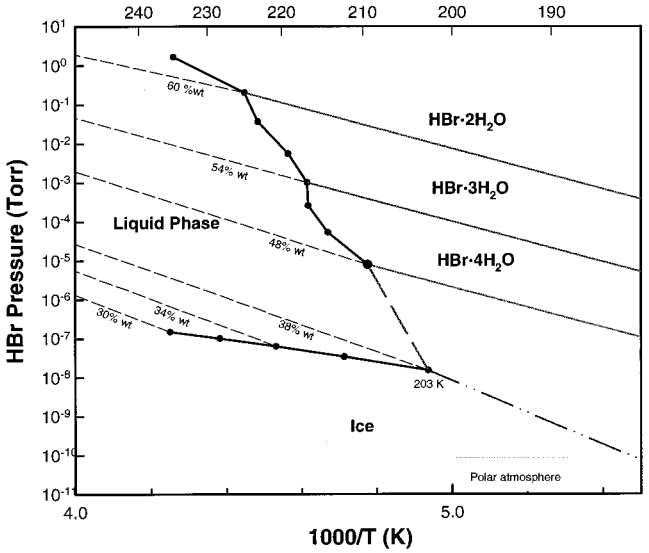

Figure 9. Plot of HBr phase diagram in terms of the partial HBr pressures and the reciprocal temperatures. A dark dashed-coexistence line assumes that the hydrate is in equilibrium with a pentahydrate as described in the text. An "ice" phase domain is included and the PSC conditions are within the "ice" phase which indicates that hydrates are unlikely to be formed on a type II PSC surface.

the HBr−ice phase diagram in Figure 9 to reflect stratospheric temperatures and partial HBr pressures. We also assume that a hydrate, $HBr{\cdot}5H_2O$, is in equilibrium with the $HBr{\cdot}4H_2O$ crystal and the ice phase at 38 wt % of the solution. Theoretically, the phase region between 38 and 47 wt % should be filled by a hydrate or hydrates. If one simply estimates the composition on the basis of the bulk solution phase at 47 wt %, $HBr{\cdot}5H_2O$ is the natural choice. Pickering theorized that this 38−47 wt % gap might perhaps be filled up by the crystallization of the pentahydrate if adequate cooling were adopted.[27] However, Pickering did not obtain $HBr{\cdot}5H_2O$ crystals in his measurements. The freezing envelope used in Figure 4 is also recommended by the *Gmeline Handbook*.[53] For the composition less than or equal to 38 wt %, it is the ice phase. Using the HBr vapor pressure at the triple point, the heat of sublimation of ice (50.93 kJ/mol at 200 K[36]), and the heat of sublimation of $HBr{\cdot}5H_2O$ (eq 14), the coexistence line between the $HBr{\cdot}5H_2O$ and ice can be calculated and is illustrated by the double dot−dash line in Figure 9. Note, that the composition of the hydrate changes the slope of this line *slightly*. The general profile of this assumed $HBr{\cdot}5H_2O$ is correct.

With the information provided in the previous paragraph, it is possible to comment on the thermodynamic state of HBr in the polar stratosphere. The shaded area in Figure 9 indicates polar stratospheric conditions. It shows that hydrobromic acid hydrates are *not likely* to form under the polar stratospheric conditions, because the gas-phase HBr concentration is too low. Similarly, one can predict the chemical properties of HBr in the upper troposphere where the concentration of bromine species is slightly higher. It is expected that HBr (∼ppt) is adsorbed near the ice cloud surface in an ionic form at about 240 K (polar region). The results of this study may be extrapolated to troposphere conditions to address the boundary-layer ozone depletion problem. As a precaution, there are indeed a few uncertainties in the HBr−ice phase diagram. Detailed thermodynamic measurements are necessary to map out the entire solid-phase region of interest to polar chemistry.

V. Summary

The principal conclusion from this study is that HBr forms both the dihydrate and trihydrate near an ice film surface at $P_{HBr} = 10^{-6}-10^{-7}$ Torr and 188−195 K. Hydrobromic acid hydrate may not be expected to form under polar stratospheric conditions according to the constructed HBr−ice phase diagram. Even if this is the case, PSCs would efficiently scavenge HBr in the atmosphere. The uptake of HBr on ice is a function of partial HBr pressure and is independent of the total pressure of the system. The uptake strongly depends on ice film thickness and morphology. The co-uptake of HBr and HCl on ice films shows that HBr, in general, is more efficiently incorporated into ice than HCl at lower temperatures. The interactions between HBr and ice or HCl and ice are stronger than that between HBr and HCl.

Acknowledgment. We thank L. F. Keyser for his constructive comments on the manuscript. We are grateful for discussion with J. P. Devlin, M. J. Molina, and D. R. Worsnop and appreciate that S. W. Benson brought our attention to reference 37. The authors also thank an anonymous reviewer for helpful comments on the manuscript. This work was supported by the National Science Foundation under grant ATM-9530659.

References and Notes

(1) Wofsy, S. C.; McElroy, M. B.; Yung, Y. L. *Geophys. Res. Lett.* **1975**, *2*, 215.
(2) Yung, Y. L.; Pinto, J. P.; Watson, R. T.; Sander, S. P. *J. Atm. Sci.* **1980**, *37*, 339.
(3) Lary, D. J. *J. Geophys. Res.* **1996**, *101*, 1505.
(4) WMO. *Scientific Assessment of Ozone Depletion: 1994*; WMO: Geneva, Switzerland, 1995.
(5) Wayne, R. P. *Chemistry of Atmospheres*, 2nd ed.; Clarendon Press: Oxford, 1991.
(6) Solomon, S.; Garcia, R. R.; Rowland, F. S.; Weubbles, D. J. *Nature* **1986**, *321*, 755.
(7) Farman, J. C.; Gardiner, B. G.; Shanklin, J. D. *Nature* **1985**, *315*, 207.
(8) Solomon, S. *Rev. Geophys.* **1988**, *26*, 131.
(9) Hanson, D. R.; Ravishankara, A. R. *Geophys. Res. Lett.* **1995**, *22*, 385.
(10) Danilin, M. Y.; McConnell, J. C. *J. Geophys. Res.* **1995**, *100*, 11237.
(11) Lary, D. J.; Chipperfield, M. P.; Toumi, R.; Lenton, T. *J. Geophys. Res.* **1996**, *101*, 1489.
(12) Barrie, L. A.; Bottenheim, J. W.; Schnell, R. C.; Crutzen, P. J.; Rasmussen, R. A. *Nature* **1988**, *334*, 138.
(13) McConnell, J. C.; Henderson, G. S.; Barrie, L.; Bottenheim, J.; Niki, H.; Langford, C. H.; Templeton, E. M. J. *Nature* **1992**, *355*, 150.
(14) Fan, S.-M.; Jacob, D. J. *Nature* **1992**, *359*, 522.
(15) Hanson, D. R.; Ravishankara, A. R. *J. Phys. Chem.* **1992**, *96*, 9441.
(16) Abbatt, J. P. D. *Geophys. Res. Lett.* **1994**, *21*, 665.
(17) Chu, L. T.; Heron, J. W. *Geophys. Res. Lett.* **1995**, *22*, 3211.
(18) Delzeit, L.; Rowland, B.; Devlin, J. P. *J. Phys. Chem.* **1993**, *97*, 10312.
(19) Gilbert, A. S.; Sheppard, N. *J. Chem. Soc., Faraday Trans. 2* **1973**, *69*, 1628.
(20) Lundgren, J.-O. *Acta Cryst.* **1970**, B*26*, 1893.
(21) Rieley, H.; Aslin, H. D.; Haq, S. *J. Chem. Soc., Faraday Trans.* **1995**, *91*, 2349.
(22) Chu, L. T. *J. Vac. Sci. Technol. A.* **1997**, *15*, 201.
(23) Chu, L. T.; Leu, M.-T.; Keyser, L. F. *J. Phys. Chem.* **1993**, *97*, 7779.
(24) Keyser, L. F.; Leu, M.-T. *J. Colloid Interface Sci.* **1993**, *155*, 137.
(25) Hanson, D. R.; Mauersberger, K. *J. Phys. Chem.* **1990**, *94*, 4700.
(26) Tompkins, F. C. *Chemisorption of Gases on Metals*; Academic Press: New York, 1978; pp 101−103.
(27) Pickering, S. U. *Philos. Mag.* **1893**, *36*, 111.
(28) *International Critical Tables of Physics, Chemistry and Technology*; McGraw-Hill: New York, 1929; Vol. 3, pp 306; Vol. 5, p 177.
(29) Haase, R.; Naas, H.; Thumm, H. *Zeit. Phys. Chemie Frankfurt* **1963**, *37*, 210.
(30) Carslaw, K. S.; Clegg, S. L.; Brimblecombe, P. *J. Phys. Chem.* **1995**, *99*, 11557.
(31) Lide, *CRC Handbook of Physics and Chemistry*, 67th ed.; CRC Press: Boca Raton, 1995; pp 5−63.

(32) Chase, M. W. J.; Davies, C. A.; Donney, J. R., Jr.; Frurip, D. J.; McDonald, R. A.; Syverud, A. N. *JANAF Thermochemical Tables*, 3rd ed.; American Chemical Society: Washington, DC, 1985; Part 1, p 430; Part 2, p 1274.

(33) Davidson, N. *Statistical Mechanics*; McGraw-Hill: New York, 1962; pp 368−371.

(34) Lord, R. C.; Ahlberg, J. E.; Andrews, D. H. *J. Chem. Phys*. **1937**, *5*, 649.

(35) Blue, R. W. *J. Chem. Phys*. **1954**, *22*, 280.

(36) Wooldridge, P. J.; Zhang, R.; Molina, M. J. *J. Geophys. Res*. **1995**, *100*, 1389.

(37) Hisham, M. W. M.; Benson, S. W. In *From Atoms to Polymers Isoelectronic Analogies*; Liebman, J. F., Greenberg, A., Eds.; VCH: New York, 1989; Chapter 9.

(38) Worsnop, D. R.; Fox, L. E.; Zahniser, M. S.; Wofsy, S. C. *Science* **1993**, *259*, 71.

(39) Haynes, D. R.; Tro, N. J.; George, S. M. *J. Phys. Chem*. **1992**, *96*, 8502.

(40) Keyser, L. F.; Moore, S. B.; Leu, M.-T. *J. Phys. Chem*. **1991**, *95*, 5496.

(41) Keyser, L. F.; Moore, S. B.; Leu, M.-T. *J. Phys. Chem*. **1993**, *97*, 2800.

(42) Kolb, C. E.; Worsnop, D. R.; Zahniser, M. S.; Davidovits, P.; Keyser, L.; Leu, M.-T.; Molina, M. J.; Hanson, D. R.; Ravishankara, A. R.; Williams, L. R.; Tolbert, M. A. In *Progress and Problems in Atmospheric Chemistry*; Barker, J. R., Ed.; World Scientific: New Jersey, 1995; Chapter 18.

(43) Gertner, B. J.; Hynes, J. T. *Science* **1996**, *271*, 1563.

(44) Hobbs, P. V. *Ice Physics*; Clarendon Press: Oxford, 1974; Chapter 1.

(45) Somorjai, G. A. *Chemistry in Two Dimensions Surfaces*; Cornell University Press: Ithaca, 1981; pp 30−33.

(46) Chu, L.; Chu, L. T. *J. Phys. Chem.*, in press.

(47) Allanic, A.; Oppliger, R.; Rossi, M. *J. Geophys. Res*. **1997**, *102*, 23529.

(48) Chu, L.; Chu, L. T. *J. Phys. Chem.*, to be submitted.

(49) Abbatt, J. P. D.; Beyer, K. D.; Fucaloro, A. F.; McMahon, J. R.; Wooldridge, P. J.; Zhang, R.; Molina, M. J. *J. Geophys. Res*. **1992**, *97*, 15819.

(50) Hanson, D. R.; Ravishankara, A. R. *J. Phys. Chem*. **1992**, *96*, 2682.

(51) Johnson, D. G.; Traub, W. A.; Chance, K. V.; Jucks, K. W. *Geophys. Res. Lett.* **1995**, *22*, 1373.

(52) Carlotti, M.; Ade, P. A. R.; Carli, B.; Ciarpallin, P.; Cortesi, U.; Griffin, M. J.; Lepri, G.; Mencaraglia, F.; Murray, A. G.; Nolt, I. G.; Park, J. H.; Radostitz, J. V. *Geophys. Res. Lett.* **1995**, *22*, 3207.

(53) *Gmelins Handbuch der anorganschem Chemie*; Verlag Chemie: Berlin, 1931; Vol. 7, pp 214.